




Cite this: *Nanoscale*, 2017, **9**, 9190

Hypoxia-induced tumor cell resistance is overcome by synergistic GAPDH-siRNA and chemotherapy co-delivered by long-circulating and cationic-interior liposomes

Jibin Guan,^{a,b} Jin Sun,^a Feilong Sun,^b Bo Lou,^b Dong Zhang,^a Vida Mashayekhi,^b Negar Sadeghi,^b Gert Storm,^b Enrico Mastrobattista^{*b} and Zhonggui He ^{*a}

Chemotherapeutic drug resistance of tumor cells under hypoxic conditions is caused by the inhibition of apoptosis by autophagy and drug efflux via adenosine triphosphate (ATP)-dependent transporter activation, among other factors. Here, we demonstrate that disrupting glyceraldehyde-3-phosphate dehydrogenase (GAPDH) expression can reduce the autophagy and ATP levels in tumor cells. To test whether GAPDH knockdown is sufficient to overcome drug resistance, a nanocarrier (asymmetry-membrane liposome) was designed to encapsulate GAPDH-siRNA with a low dose of paclitaxel (PTX). Liposomes were prepared using novel cryogenic inner-outer dual reverse phase emulsion liposome manufacturing technology to obtain a high loading of siRNA. The results of dynamic light scattering (DLS) indicated that the liposomes had an average hydrodynamic diameter of 250.5 nm and polydispersity index (PDI) of 0.210, which was confirmed by (Transmission Electron Microscope) TEM images. In *in vitro* tests, the siRNA liposomes presented a high specificity in the suppression of GAPDH expression and significant synergy in cytotoxicity with co-delivery of PTX against tumor cells (HeLa and MCF-7) under hypoxic conditions. Moreover, *in vivo* studies (a HeLa tumor xenograft model using female BALB/c nude mice) demonstrate that the liposomes could not only increase the concentration of drugs in tumors over time but also successfully boosted the chemotherapeutic efficacy of PTX (synergistic therapy with GAPDH-siRNA). Tumor cells appeared to lose their resistance against PTX therapy, becoming more sensitive to PTX when GAPDH-siRNA was simultaneously administered in long-circulating liposomes. Consequently, the novel delivery of GAPDH-siRNA using nanotargeted liposomes provides a useful and potential tool to overcome multidrug resistant (MDR) tumors and presents a bright prospect compared with the traditional chemotherapeutic strategies in clinic cancer therapy.

Received 14th April 2017,

Accepted 1st June 2017

DOI: 10.1039/c7nr02663c

rs.c.li/nanoscale

1. Introduction

The multidrug resistance (MDR) of cancer cells limits the efficacy of clinical chemotherapy. Overexpression of ATP binding cassette (ABC) transporters such as P-glycoprotein makes tumor cells resistant to many conventional chemotherapeutic drugs such as paclitaxel (PTX), doxorubicin (Dox) and cisplatin.^{1,2} Recent research indicates that hypoxia-inducible factor (HIF-1 α) in cancer cells increases their energy metabolism and ATP synthesis to satisfy the high demand

for ABC transporters.³ Hence, targeting and suppressing ATP production in hypoxic tumor cells could be used to reduce cellular resistance to drugs and enhance the efficacy of chemotherapy.

With the strategy of targeting ATP production, we focused on cellular glycolysis. This pathway is the major energy provider of anoxic cells, which are often found at the core of rapidly growing solid tumors. Under hypoxic conditions, GAPDH up-regulation leads to increased levels of cytosolic ATP, which in turn activates the ABC transporter.^{4,5} Additionally, GAPDH up-regulates autophagy to limit apoptotic cell death and increase the survival of tumor cells.⁶ Therefore, the down-regulation of GAPDH is likely to lead to reduced ATP levels and decrease the MDR of hypoxic tumor cells. As a result, tumor cells would undergo apoptosis and be more sensitive to chemotherapy drug after disrupting GAPDH expression by RNAi, which could be a valuable option in future chemotherapeutic strategies.

^aDepartment of Pharmaceutics, School of Pharmacy, Shenyang Pharmaceutical University, Shenyang 110016, PR China. E-mail: hezhonggui@vip.163.com;

Fax: +86-24-23986321; Tel: +86-24-23986321

^bDepartment of Pharmaceutics, Utrecht Institute for Pharmaceutical Sciences, University of Utrecht, 3584CG, The Netherlands. E-mail: E.Mastrobattista@uu.nl;

Fax: +31 30 251 7839; Tel: +31 (0)62 273 6567

Among recent studies of RNAi carriers, viral vectors (*i.e.*, retroviruses, lentivirus, and adenoviruses) are a short hairpin RNA (shRNA) delivery transporter with a high efficiency of transfection. However, they have a limited loading capacity and severe immune responses as well as oncogenic potential.⁷ Cationic polymers such as polyethylenimine (PEI),^{8–10} poly-amidoamine dendrimer (PAMAM),^{11,12} and chitosan^{13–15} can absorb negatively charged siRNAs by electrostatic interactions and can be prepared into nanoparticles with high encapsulation.^{16–18} However, adsorption of polycations to cell membranes may cause distortion of cell membranes and elimination by the reticuloendothelial system (RES) at the primary organs, which are significant challenges for cationic polyplexes.^{19–22} Compared with these delivery systems, co-delivery of siRNA and antitumor drugs *via* a nanocarrier^{23,24} could induce a synergistic tumor suppression effect; in particular, PEGylated liposomes²⁵ with good flexibility, biocompatibility, and encapsulating capacity, are appropriate for an ATP targeting strategy against hypoxic tumor cells.

In this work, for the first time, GAPDH-siRNA and PTX were co-delivered into hypoxic tumor cells to overcome MDR *via* synergy of ATP suppression and apoptosis activation. A long-circulating liposome with a cationic interior was developed to load hydrophilic (siRNA) and hydrophobic (PTX) compounds simultaneously for high-efficiency co-delivery owing to its unique drug delivery system with a spherical lipid bilayer. As shown in Fig. 1A, an inner monolayer lipid vesicle in which GAPDH-siRNA is loaded is covered by an outer layer with PEG to protect the asymmetrical nanocarrier, simultaneously incorporating PTX between the two layers. Additionally, the asym-

metric structure greatly helped the liposomes cover the surface charges, avoid RES clearance, and improve the accumulation of liposomes in the primary organ.^{7,26} Finally, the novel GAPDH-siRNA-PTX liposomes were targeted to tumors and endocytosed by cancer cells to cause ATP down-regulation, apoptosis activation, and tumor shrinkage.

The co-delivery system, which employs long-circulating and cationic-interior liposomes, executes the strategy of synergistically targeting GAPDH and activation of apoptosis, which is a long-awaited approach to overcome hypoxia-MDR.

2. Results and discussion

2.1 Preparation of siRNA-PTX liposomes

To obtain unilamellar liposomes with high encapsulation efficiencies of both siRNA and PTX, we used a method recently developed by Mokhtarieh *et al.*,⁷ with some modifications. This method is based on the formation of two separate w/o emulsions that, when mixed together, would form liposomes with asymmetric bilayers (Fig. 1A). To increase the stability of the emulsion that would form the interior of the liposomes during mixing and solvent evaporation, we cooled the w/o emulsion to subzero temperatures using dry ice. This resulted in solidification of the aqueous core of the inner emulsion, thereby preventing premature release of its siRNA/PTX contents to the exterior phase. As described in the particle-structure design in Fig. 1A, PEG-lipids are simply arranged at the periphery of the inner layer. TEM imaging (Fig. 1B) was used to visualize the morphology of spherical siRNA-PTX liposomes,

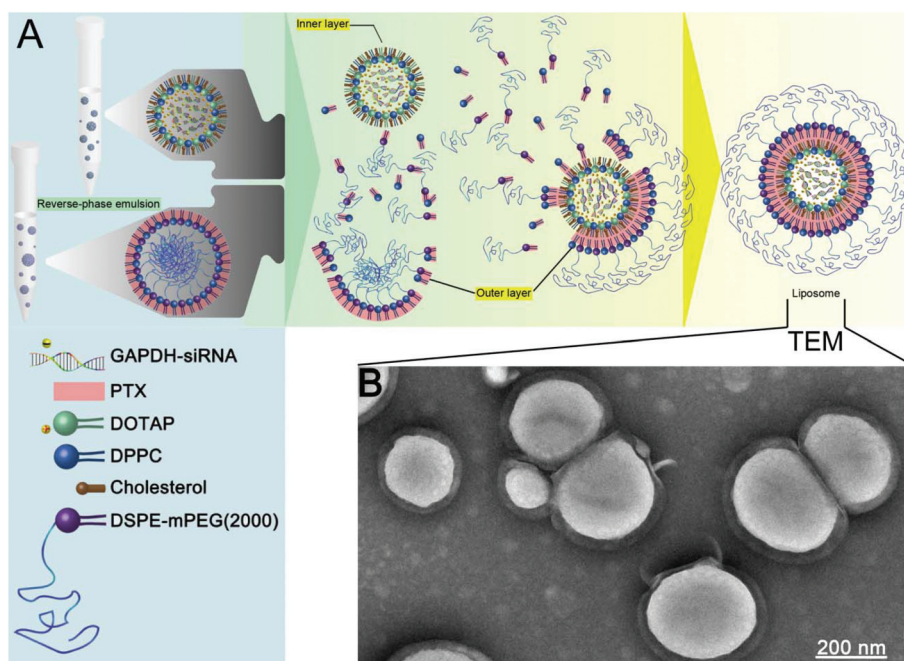


Fig. 1 Design flowsheet of the long-circulating liposome. (A) The lipid materials (DOTAP, DPPC, cholesterol, DSPE-mPEG (2000)) and drugs (GAPDH-siRNA, PTX) were showed as models in a diagram which shows the formation of the liposome from two different reverse-phase emulsions. (B) Characterization of the obtained liposomes on a TEM image (bar = 200 nm).

Table 1 The physicochemical properties of the liposomes

Physicochemical properties	Values
Mean sizes (nm)	251 ± 25 (DLS); 205 ± 9 (NTA)
PDI	0.210 ± 0.037
Zeta (mV)	0.699 ± 0.708
Encapsulation efficacy (EE%)	66.0 ± 7.6 (siRNA); 90.9 ± 2.7 (PTX)
Drug loading (DL%)	0.23 ± 0.04 (siRNA); 1.86 ± 0.02 (PTX)

Table 2 Models of drug release

Model name	Equation
Zero-order model	$Q_t = k_0 \cdot t$
First-order model	$\ln(Q_0 - Q_t) = -k_1 \cdot t + \ln Q_0$
Higuchi diffusion model	$Q_t = k_H \cdot t^{1/2}$

and the outer face of the sphere was found to present a thin hydrated PEG layer, which was different from the inner structure. A description of the liposomes' physicochemical properties is shown in Table 2. The zeta potential (0.699 mV) indicated that the formed liposomes had an electroneutral PEG encircled surface. Given the lipid composition, one would expect a positive zeta potential if the lipids were equally distributed over the inner and outer layer of the lipid membrane. The neutral charge measured strongly suggested an asymmetric distribution of the bilayer with an electropositive inner layer attracting the electronegative siRNA and loaded PTX. Because of this strong electrostatic interaction, the encapsulation efficiencies of siRNA and PTX could reach up to 66.0% and 90.9%, respectively. The morphology of the spherical siRNA-PTX liposomes was visualized using TEM (Fig. 1B). The average size and size distribution of the liposomes were determined by DLS (size distribution by scattering intensity) and NTA (size distribution by number) analyses. The results were 250.5 nm with PDI at 0.210 (DLS) and 204.8 nm (NTA). The difference between the results of the two size measuring methods could be attributed to the fact that DLS calculates the average particle size by measuring fluctuations in scattering intensity and is profoundly affected by the presence of a few large particles.²⁷

2.2 Drug release

As shown in Fig. 2, Taxol exhibited relatively fast release of PTX, and the cumulative release was more than 90% within 24 h. In contrast, less than 50% PTX was released from liposomes into the medium over the same time. The slow release profile illustrated that the stability of liposomes under pH 7.4 conditions could prevent drug leakage during the delivery process.

For the kinetics model of the liposomes, the release mechanism was investigated using three main equations, as shown in Table 3: the zero-order release equation, the first-order release equation²⁸ and the Higuchi equation²⁹ were used to match formulations release process. The results showed that the *in vitro* release behavior of both Taxol and the liposomes

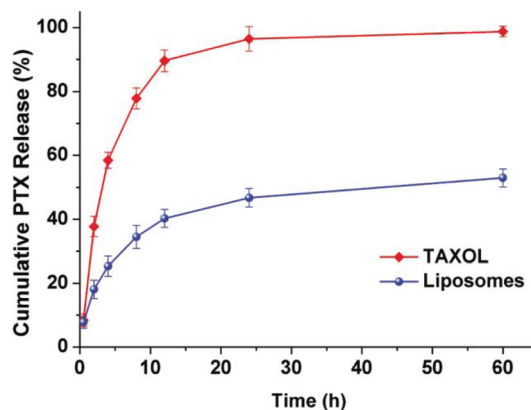


Fig. 2 Cumulative PTX release from Taxol and liposomes in PBS (pH 7.4) containing 20% (v/v) ethanol and incubated with gentle shaking (100 rpm) from 0.5 to 60 h at 37 ± 0.5 °C. Each value indicates the mean ± standard deviation and is representative of results obtained from three independent experiments ($n = 3$).

Table 3 Hemolysis percentages of Taxol and siRNA-PTX liposomes at different concentrations

	Absorbance (A)	Hemolysis (%)
Taxol with 0.6 mg per mL PTX	0.132 ± 0.005	27.54 ± 1.072
Taxol with 0.3 mg per mL PTX	0.015 ± 0.003	1.36 ± 0.615
Liposome with 0.6 mg per mL PTX	0.022 ± 0.001	2.85 ± 0.236
Liposome with 0.3 mg per mL PTX	0.014 ± 0.001	1.09 ± 0.257
Negative control	0.009 ± 0.001	—
Positive control	0.458 ± 0.008	—

was close to the first-order release equation ($r^2 = 0.9801$ and 0.9694, respectively).

2.3 Cell uptake

Alexa Fluor® 647 labelled siRNA and coumarin-6 were used as GAPDH-siRNA and PTX for fluorescence imaging, respectively. As shown in Fig. 3, with similar quantification data as Alexa Fluor® 647, the coumarin-6 fluorescence intensity (IOD/area) of the free drug solution group was significantly lower than that of the liposome group, indicating that the cellular uptake of the free drug solution was lower than that of the liposomes. Transversal slice images showed that the drug was internalized and not bound to the surface of the cells. These results of CLSM analysis suggest that the liposomes could successfully accumulate in tumor cells *via* cell endocytosis uptake.

To elucidate the uptake mechanism, PEGylated nanoliposomes were used in the HeLa cells. As shown in Fig. 4, colchicine could inhibit the formation of macropinosomes. Besides, quercetin is the inhibitor of clathrin- and caveolae-independent endocytosis. Therefore, the negative results of quercetin and colchicine indicated that the uptake pathways of the liposomes did not include macropinocytosis and clathrin-caveolae independent endocytosis. Meanwhile, chlorpromazine can disrupt clathrin from the cell membrane to inhibit clathrin-dependent endocytosis.³⁰ After being pretreated with chlorpro-

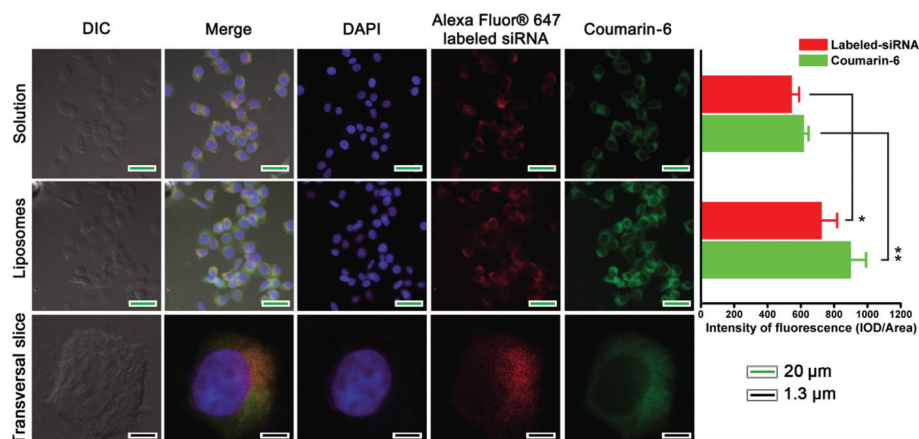


Fig. 3 Fluorescent quantitation analyses on cellular uptake of siRNA-PTX liposomes. The scale bar is 10 μm (green) and 1.3 μm (black). The siRNA and PTX were mixed with Alexa Fluor® 647 labeled siRNA (red) and coumarin-6 (green), respectively. Both of the mixing ratios of the two fluorescent probes were 10%. Cell nuclei were stained with 4',6-diamidino-2-phenylindole (DAPI; blue). Left: CLSM images of the siRNA-PTX solution and liposomes uptake in HeLa cells. Right: Fluorescent quantification analysis histogram of CLSM data on internalization of Alexa Fluor® 647 and coumarin-6, which showed the solution and liposomes against HeLa cells. The fluorescence intensity (IOD/area) was measured by using Nikon Instruments software ($n = 3$, $*p < 0.05$, $**p < 0.01$).

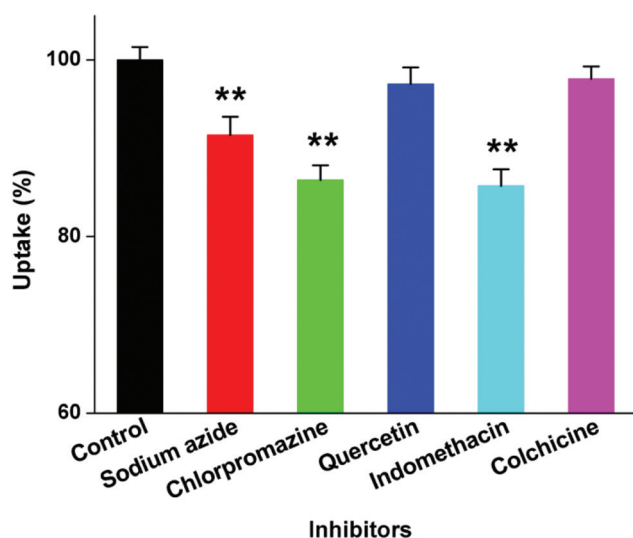


Fig. 4 Statistics of flow cytometry for calculating the effect of endocytic inhibitors on cellular uptake in HeLa cells. The cells were pre-treated with different inhibitors (3 μg per mL sodium azide, 10 μg per mL chlorpromazine, 6 μg per mL quercetin, 6 μg per mL indomethacin and 8 μg per mL colchicine), then co-incubated with siRNA-PTX/coumarin-6 liposomes for 2 h at 37 ± 0.5 $^{\circ}\text{C}$. The concentration of coumarin-6 was 3 μg mL^{-1} . Each value indicates the mean \pm standard deviation and was representative of results obtained from three independent experiments. Statistical significance relative to non-inhibitor control ($n = 3$), $*p < 0.05$, $**p < 0.01$.

mazine and then treated with siRNA-PTX/coumarin-6 liposomes, the cellular uptake of the drugs was decreased to 86% compared with the control group without any inhibitor. Similarly, when pre-incubated with a caveolin-dependent endocytosis inhibitor of indomethacin,³¹ cellular uptake was reduced to 85%, suggesting that both clathrin and caveolin

dependent endocytosis perhaps take part in the uptake of the liposomes. Upon pre-incubation with sodium azide, the cellular uptake was significantly reduced to 91%. Therefore, the results demonstrate that the uptake of high-PEGylated liposomes is an energy-dependent endocytosis process *via* clathrin- and caveolin-mediated pathways.

2.4 Transfection

GAPDH enzyme activity assays of HeLa and MCF-7 cells were performed and are shown in Fig. 5. Compared with the negative control siRNA, the liposome group had a similar specificity for gene silencing efficiency as the Lipofectamine 2000® lipoplexes group. Additionally, the dose-response curve showed that as the concentrations of siRNA increased, the activity showed a sharp decline. Therefore, the GAPDH-siRNA liposomes had sequence-specific effects in the two cell lines. These results indicate that the liposomes could get into cells *via* endocytosis and release a specific siRNA to inhibit the expression of the target gene (GAPDH).

2.5 *In vitro* cytotoxicity studies

The cell viability of HeLa and MCF-7 cells incubated with siRNA liposomes for 24 h was above 80%, as shown in Fig. 6, demonstrating the safety of the vector and siRNA. The biological activity of PTX and siRNA released from different formulations was evaluated by the MTS assay. The survival rate of cells incubated with liposomes and Taxol showed PTX dose-dependent cytotoxicity at a series of PTX concentrations from 0.001 to 10 μg mL^{-1} . However, the cell survival rate under normal culture conditions was higher than that under hypoxic conditions. This indicates that PTX could induce acute drug resistance in the tumor cells under hypoxic conditions, in agreement with a report by Bhattacharya³² showing that

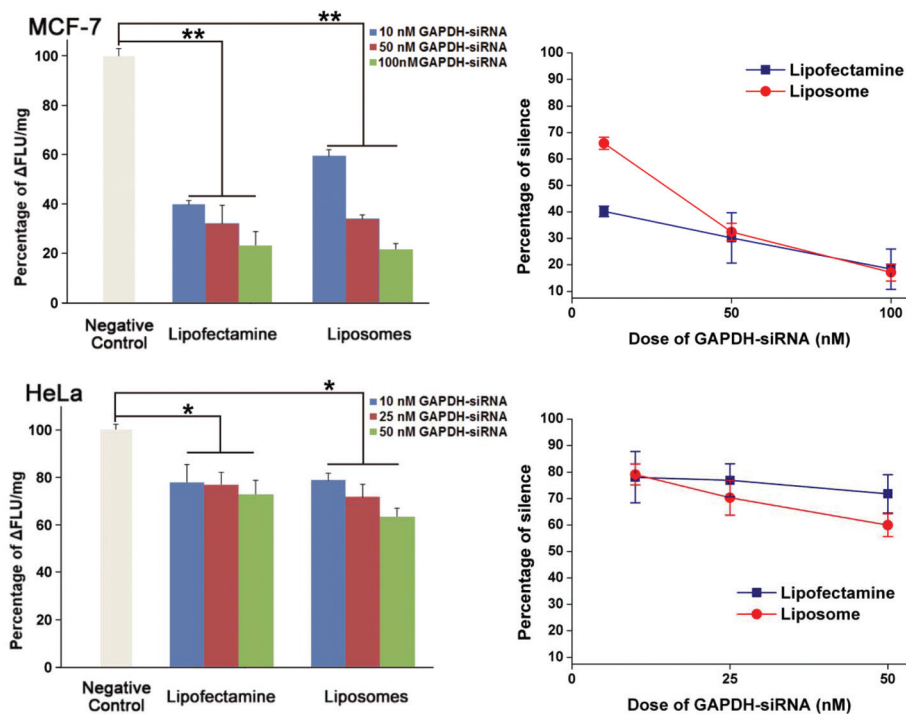


Fig. 5 GAPDH enzyme activity assay after the transfection with lipoplexes (Lipofectamine) and liposomes with GAPDH-siRNA concentrations of 10 nM, 25 nM, 50 nM and 100 nM against MCF-7 and HeLa cells. After 48 h transfection for GAPDH siRNA-transfected cultures, the remaining GAPDH expression was calculated as a percentage of negative control (treated with no-target siRNA). Each value indicates the mean \pm standard deviation and was representative of results obtained from three independent experiments. Statistical significance relative to negative control siRNA ($n = 3$), $p < 0.05$ is denoted by * and $p < 0.01$ by **.

hypoxic conditions induce tumor cells to become drug resistant. However, the siRNA-PTX administration caused a higher cytotoxicity than PTX administration alone under hypoxic conditions, indicating that GAPDH knockdown can promote the sensitivity of tumor cells to PTX.

2.6 The mechanism involved in the reduction of multiple drug resistance (MDR) by GAPDH knockdown

The HeLa cells were incubated with HBS, Cremophor EL, Taxol, empty liposomes, siRNA liposomes, PTX liposomes and siRNA-PTX liposomes. After 24 h, the expression of autophagy (Atg-5, Atg-12) and apoptosis (caspase-3) proteins in both hypoxic and standard culture environments were evaluated by western blotting to detect the dynamic variation and the relationship between apoptosis and autophagy. Atg-5 and Atg-12 are expressed when autophagy is activated since they are crucial for the formation of the autophagosome. As a critical executioner of apoptosis, caspase-3 expression indicates completely activated apoptosis. Western blots under standard conditions (Fig. 7) show that no group had increased autophagy protein expression, indicating that GAPDH knockdown and stabilization of microtubule polymers did not activate the autophagy pathway. However, Taxol, PTX liposomes and siRNA-PTX liposomes groups had increased caspase-3 and cleaved caspase-3 expression. This suggests that all PTX could induce apoptosis. Under hypoxic conditions, only Taxol and PTX liposome groups showed increased expression of Atg-5

and Atg-12, but decreased expression of caspase-3, indicating that the cells switched from autophagy to apoptosis when administered PTX under hypoxic conditions. Therefore, tumor cells could maintain survival *via* autophagy and showed a PTX resistant phenomenon in the cell cytotoxicity assay under hypoxic conditions. Nevertheless, under these conditions, the siRNA-PTX liposome-treated cells not only did not show increased expression of autophagy proteins but also showed induction of apoptosis. Additionally, the apoptosis pathway of tumor cells with knockdown of GAPDH expression was not influenced by hypoxic conditions. GAPDH-siRNA could therefore assist PTX therapy by combating the tumor cells resistance caused by hypoxia.

Since the apoptotic cells release ATP³³ and some of the released ATP is degraded or depleted, the ATP level of PTX and siRNA-PTX administered cells declined compared with the control group (Fig. 8). In contrast, PTX-treated cells under hypoxic conditions, which showed increased autophagy, had similar ATP levels as the control cells, indicating that autophagy and anaerobic glycolysis could maintain cell ATP levels, which could promote PTX resistance under hypoxic conditions. Anaerobic glycolysis is the leading ATP-producing pathway (converting glucose to lactate) for cells in a hypoxic environment. Furthermore, GAPDH is an essential enzyme in that pathway to catalyze glyceraldehyde 3-phosphate to D-glycerate 1,3-bisphosphate. Therefore, as Fig. 8 shows, GAPDH knockdown (using siRNA liposomes transfection) significantly reduces cell ATP

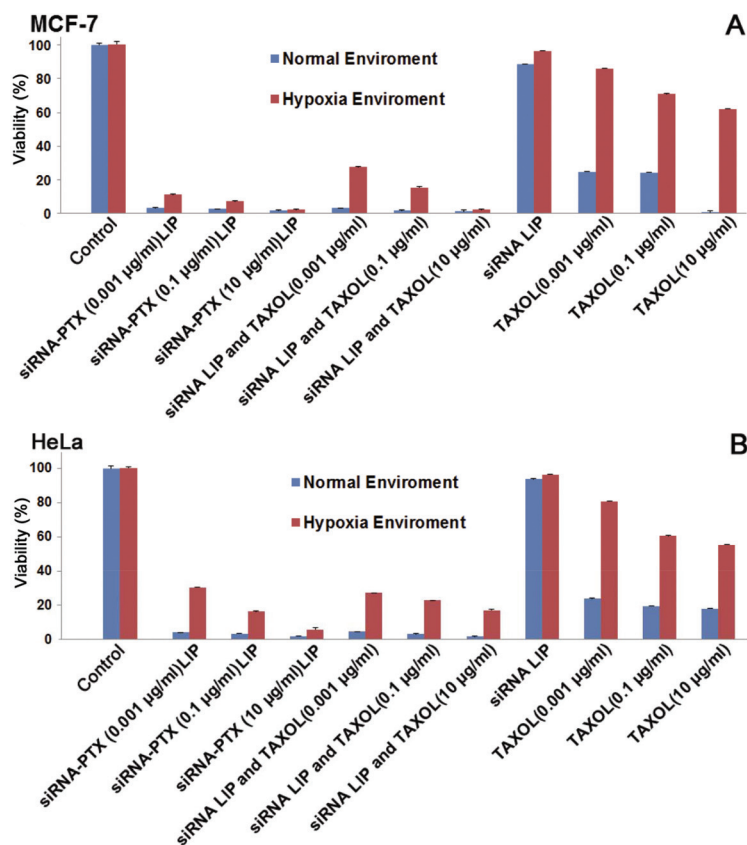


Fig. 6 Cell viability histogram (mean \pm standard deviation, $n = 3$) of the MTS assays against MCF-7 (A) and HeLa (B) cells after 24 h treatment with various formulations. The concentrations of siRNA were fixed at 50 nM, and the concentrations of PTX were gradually increased from 0.001 to 10 $\mu\text{g ml}^{-1}$.

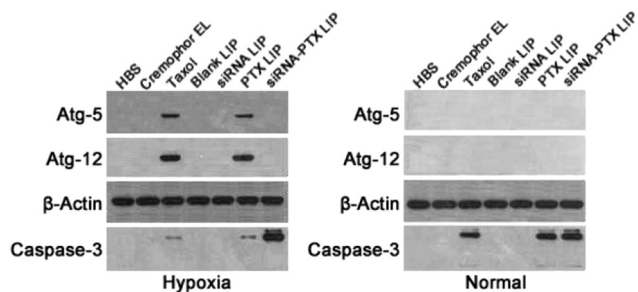


Fig. 7 Autophagic and apoptotic study of Cremophor EL, Taxol, blank liposomes, siRNA liposomes, PTX liposomes and siRNA-PTX liposomes against HeLa cells. Protein expression levels of Atg-5, Atg-12, caspase-3 and cleaved caspase-3 after treatment with different siRNA, PTX and blank formulations for 24 h. Cells with the treatment of normal saline (NS) were used as a negative control. β -Actin (42 kDa) was used as a loading control.

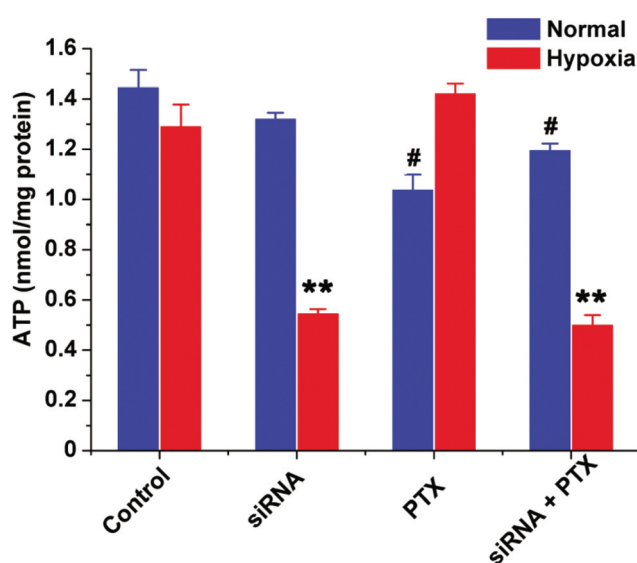


Fig. 8 The effects of siRNA, PTX and siRNA-PTX liposomes on the intracellular ATP level in HeLa cells after normal and hypoxia incubation respectively. Data are presented as the mean \pm standard deviation and representative of results obtained from three independent experiments ($n = 3$). Statistical significance relative to hypoxia control (red), * $p < 0.05$ and ** $p < 0.01$. Statistical significance relative to normal control (blue), # $p < 0.05$ and ## $p < 0.01$.

levels under hypoxic conditions. Furthermore, Zhang *et al.*³⁴ reported that the expression of ATP-dependent membrane transporter proteins in cancer cells is considered to be the primary cause of MDR. Thus, the drug efflux process could be inhibited by decreasing ATP levels. Thus, MDR would be reduced by GAPDH knockdown in tumor cells.

2.7 *In vivo* drug biodistribution

DiR was used to examine the distribution of different formulations in HeLa tumor-bearing mice. After intravenous administration, the drug was visualized and calculated with a near infrared optical imaging system. As shown in Fig. 9A, the solution-treated group showed a quick elimination from 2 to 24 h. Nevertheless, the liposome-treated group displayed a longer residence time in the body. Furthermore, imaging of excised organs and tumors demonstrated that the long-circulating liposomes could target the tumor *via* an enhanced permeation and retention (EPR) effect. Additionally, a histogram of the fluorescence intensity showed that the accumulation of the drug in normal organs, such as the lung, which is shown in Fig. 9B, was less than in the solution-treated group, indicating that the liposomes did not cause a toxic drug reaction or significant side effects.

2.8 *In vivo* anti-tumor studies

Western blot images (Fig. 10F) were used to examine GAPDH expression in the HeLa cell line and tumors. Compared with the expression in the HeLa cell line, GAPDH was overexpressed in the HeLa xenograft tumors (a) as well as HeLa cells cultured under hypoxic condition (d). This suggests the presence of hypoxia in HeLa xenograft tumors. Furthermore, the tumors treated with siRNA liposomes (b) presented similar GAPDH levels as the HeLa cell line (c), which suggests that the liposomes could deliver siRNA to hypoxic tumor cells to suppress GAPDH overexpression.

Considering the principle of safety in applying medication, we chose to administer repeated low doses of drug in the *in vivo* assay. As shown by the hemolysis assay results, 0.3 mg per mL PTX was a safe concentration for the *in vivo* anti-tumor efficacy test.

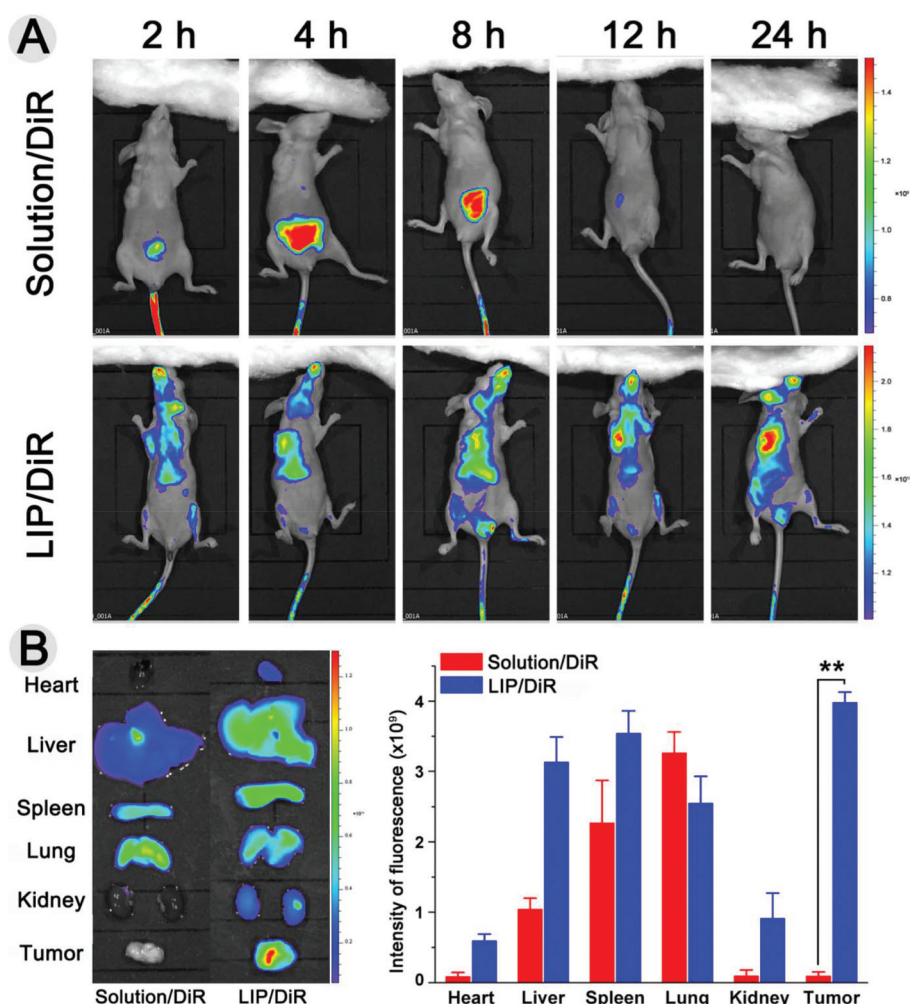


Fig. 9 Bio-distribution of DiR solution and DiR liposomes in HeLa tumor-bearing BALB/c mice. (A) *In vivo* fluorescence images of HeLa tumor-bearing mice administrated with DiR solution and DiR liposomes at different time points. (B) *Ex vivo* fluorescence images of tumors and major organs of mice euthanized at 24 h post-injection. Right of the organ images: Quantification histogram of intensity of fluorescence (IOD/area) of the organs after statistic determination and analysis. Each value indicates the mean \pm standard deviation and is representative of results obtained from three independent experiments. Statistical significance relative to vehicle control, * $p < 0.05$ and ** $p < 0.01$.

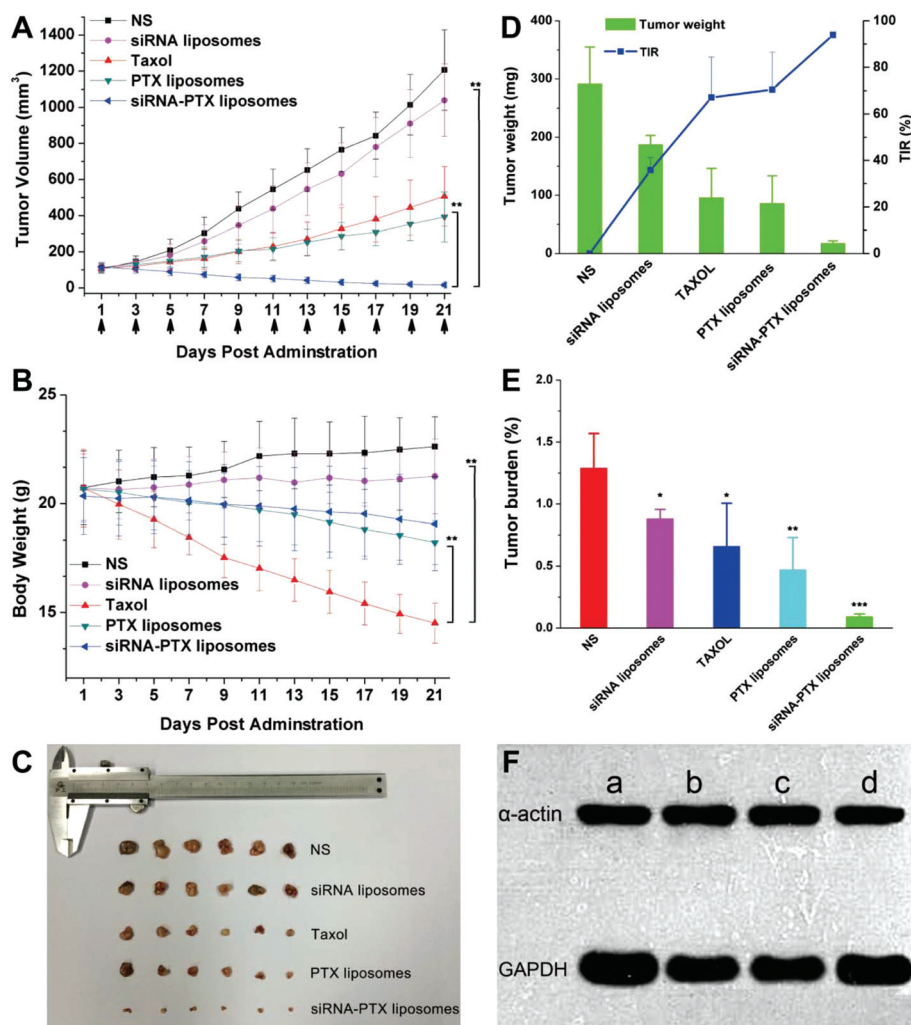


Fig. 10 *In vivo* antitumor efficiency evaluation of siRNA-PTX liposomes on HeLa tumor-bearing mice. (A) Tumor volume and (B) body weight changes after intravenous administration of saline, siRNA liposomes, Taxol, PTX liposomes and siRNA-PTX liposomes ($n = 6$). (C) The morphology of isolated tumors from HeLa tumor-bearing mice of different drug-loaded groups at the end of tests ($n = 6$). (D) Tumor weight and tumor inhibition rate (TIR) of various groups. (E) Tumor burden, the weight of tumors was divided by the average body weight of mice. (F) Western blot of GAPDH (MW: 38 kDa) expression in HeLa xenograft tumor control (a), HeLa xenograft tumor treated with GAPDH-siRNA liposomes (b), HeLa cells cultured in normal condition (c) and HeLa cells cultured in hypoxia condition (d). Alpha-actin (MW: 100 kDa) was used as a loading control. Each image of protein blots is representative of results obtained from three independent experiments ($n = 3$).

Anti-tumor efficacy was evaluated by a pharmacodynamics study. Tumor volume and body weight were measured after tail vein injection of normal saline (NS), siRNA liposomes, Taxol, PTX liposomes, and siRNA-PTX liposomes (as shown in Fig. 10A and B) to HeLa tumor-bearing mice. With 21-day treatment, all dosed groups showed tumor inhibition in different degrees compared with the NS group. As expected, almost no significant difference between the NS ($1206.8 \pm 222.1 \text{ mm}^3$ ($n = 6$, mean \pm SD)) and siRNA liposome ($1039.1 \pm 200.4 \text{ mm}^3$) groups in tumor inhibition was found, which is in agreement with the cytotoxicity assay results showing that the siRNA liposomes had no inhibition efficacy on tumor cells. The Taxol-treated group showed a moderate effect on tumor growth inhibition, with a mean tumor size of $506.9 \pm 165.2 \text{ mm}^3$. The treatment of the PTX liposomes group exhibited stronger

effects than the Taxol group, with a mean tumor size of $392.6 \pm 138.5 \text{ mm}^3$ after 15 days' administration, which was likely induced by the long circulation property and the passive targeting of tumor tissues through the EPR effect. Furthermore, and notably, the siRNA-PTX liposome group showed the greatest tumor reduction, with a mean tumor size of only $16.1 \pm 10.1 \text{ mm}^3$ (Fig. 10A). In addition, tumors were excised to calculate the tumor inhibition rate (TIR) of all treated groups (Fig. 10D). siRNA-PTX liposomes showed the strongest effect of tumor growth inhibition with 93.9% TIR. In agreement with the above *in vitro* results, the enhanced efficacy of siRNA-PTX liposome treatment largely resulted from the synergy of PTX and GAPDH knockdown.

The aim of monitoring the body weight loss of the mice, which was recorded every day after drug administration, was to

evaluate adverse drug reactions. The Taxol group showed severe weight loss in the mice, with a rapid decrease in weight after seven days, indicating serious side effects of this chemotherapeutic agent (Fig. 10B). However, the other three liposome groups had less effect on body weight, suggesting that the liposomes were less noxious than Cremophor EL and ethanol. In agreement with the hemolysis result (Table 1), PTX liposomes appeared to be safer with regard to side effects than the commercial PTX solution formulation.

3. Conclusion

In this study, siRNA-PTX liposomes with high stability were prepared using a novel microthermal inner-outer dual reverse phase emulsion method. The prepared liposomes showed tumor accumulation after intravenous administration. In accordance with the *in vitro* cytotoxicity studies, repeated low dose injections with siRNA-PTX liposomes showed a prominent chemotherapeutic efficacy and low systemic toxicity. As a highly efficient drug delivery system, the long-circulating stealth PTX liposomes could simultaneously load GAPDH-siRNA into tumor cells to promote PTX-induced apoptosis by inhibiting the hypoxia-dependent autophagy induced MDR. In summary, these results suggest that low dose chemotherapy combined with GAPDH knockdown is a promising strategy for reducing MDR to improve the efficiency of cytostatics in clinical cancer therapy.

4. Materials & methods

4.1 Materials

Chemically modified GAPDH-siRNA (sense strand, 5'Hy-mG-rG-mU-rC-mA-rU-mC-rC-rA-rU-rG-rA-mC-rA-mA-rC-mU-rU-mU-dT-PS-dT-Hy3' and antisense strand, 3'Hy-dT-PS-dT-mC-rC-mA-rG-mU-rA-mG-rG-rU-rA-rC-mU-rG-mU-rU-mG-rA-mA-rA-Hy5'), no-target siRNA-1(D-001810-01) and Alexa Fluor®647 labelled siRNA (sense strand, 5'Hy-rA-rU-mC-rG-mU-rA-mC-rG-mU-rA-mC-rC-rG-mU-rC-rG-mU-rA-mU-PS-dT-PS-dT-Hy3' and antisense strand, 3'Hy-dT-PS-dT-PS-mLJ-rA-rG-mC-rA-mU-rG-mC-rA-mLJ-rG-rG-mC-rA-rG-mC-rA-mU-rA-Hy5') were obtained from Dharmacon Bioscience (Lafayette, USA). Paclitaxel (PTX) was purchased from Dalian Meilun Biology Technology Co. Ltd (China). DSPE-PEG2000 was obtained from Shanghai Advanced Vehicle Technology Pharmaceutical Ltd (Shanghai, China). DPPC, DOTAP and cholesterol were from Sigma-Aldrich (St Louis, MO, USA). Cremophor® EL was purchased from Sigma-Aldrich (St Louis, MO) and used to produce the formulation of PTX according to the commercial Taxol. Near infrared lipophilic carbocyanine dye 1,1'-dioctadecyltetramethyl indotricarbocyanine iodide (DiR) was purchased from Fanbo Biochemical (Beijing, China). Antibodies against Atg-5, Atg-12, caspase-3 and β -actin were purchased from Cell Signaling Technology, Inc. (Danvers, MA, USA). The Lipofectamine 2000® transfection kit (Invitrogen, Carlsbad, CA) and ATP test kit (Beyotime®

Biotechnology Co., Ltd, Nantong, China) were used according to the supplied protocols. Dulbecco's modified Eagle's medium (DMEM) and trypsin were from Sigma-Aldrich (St Louis, MO, USA). MTS assay kits were obtained from Promega Corporation (Madison, USA). All reagents and compounds were used without further purification or modification.

4.2 Preparation of siRNA-PTX liposomes

Lipids for the inner layers and lipids for the outer layers mixed with PTX were weighed and dissolved in 2–3 mL chloroform in two flasks respectively (inner layer: DPPC 18 mM and DOTAP 9 mM; outer layer: DPPC 27 mM, PEG2000-PE 6 mM, and cholesterol 30 mM). The total lipids were composited under a proper molar ratio (DPPC, DSPE-PEG, DPTAP, cholesterol as 15 : 2 : 3 : 10). The chloroform was removed by rotary evaporation and under nitrogen blowing. The film (outer) was hydrated with 0.2 mL HBS (10 mM, pH 7.4) and then transferred into a tube, where 0.6 mL diethyl ether and 0.1 mL ethanol were added. The film (inner) was hydrated with siRNA solution (dissolved 10 mM sodium citrate, pH 4.0) and transferred into a tube, and then 0.4 mL diethyl ether was added. After being sonicated into emulsion respectively, the outer layer emulsion was transferred into a flask under an ice-water bath. Meanwhile, the inner layer emulsion was preserved under a dry ice-ethanol bath. After the colour of the emulsion turning white (which means the water phase inside inner layer were frozen), the inner layer emulsion was quickly transferred into another flask and mixed with outer layer emulsion. Immediately, the ether was removed by rotary evaporation, then 10 mL HBS (10 mM, pH 7.4) was added into the flask. Through a filter (0.45 μ m), the free PTX was removed from the solution. The untrapped material was removed by ultra-centrifugation at $2 \times 55\,000$ rpm for 50 min each (supernatant was removed at each centrifugation and then HBS was filled into the tube each time), and the pellet was resuspended in 3 mg PTX per 10 mL value of liposomes obtained as the final product.

For the evaluation of siRNA encapsulation in liposomes, the fluorescently labelled siRNA was used instead of general GAPDH siRNA. After damaging the lipid bilayers with 10% Triton, labelled siRNA was determined with a Jasco FP8300 Spectrofluorometer ($\lambda_{\text{excitation}} = 554$ nm; $\lambda_{\text{emission}} = 668$ nm). And the amount of encapsulated PTX was determined by the HPLC method (Hitachi HPLC system (Tokyo, Japan); mobile phase: acetonitrile–water (60 : 40, v/v); flow rate: 1 ml min⁻¹; chromatographic column: 250 \times 4.6 mm, NUCLEOSIL 100-5 C18 (Macherey-Nagel, GmbH & Co. KG, Düren Germany); detector wavelength: 227 nm).

4.3 Characterization of siRNA-PTX liposome systems

The average size and size distributions of the formed liposomes were determined by dynamic light scattering (DLS) and nanoparticle tracking analysis (NTA). DLS measurements were performed using a Malvern CGS-3 multiangle goniometer (Malvern Ltd, Malvern, UK) with a JDS Uniphase 22 mW He–Ne laser operating at 632 nm, an optical fiber-based detector and a digital LV/LSE-5003 correlator. Autocorrelation func-

tions were analysed by the cumulants method (fitting a single exponential to the correlation function to obtain the mean size and the PDI) and the CONTIN routine (fitting a multiple exponential to the correlation function to obtain the distribution of particle sizes). All measurements were performed at a 90° angle. NTA measurements were conducted with a NanoSight LM10SH (NanoSight, Amesbury, UK), equipped with a sample chamber with a 532 nm laser. The samples were injected into the sample chamber with a syringe until the liquid reached the tip of the nozzle and measured for 60 s with a manual shutter and adjustments were made. The zeta potential of the liposomes was measured by a zeta potential analyzer (Malvern Instruments, Malvern, UK) at 25 ± 0.1 °C. The morphology of the liposomes was observed by JEM 2100 transmission electron microscopy (TEM; JEOL, Japan). The samples were negatively stained with 2% phosphotungstic acid (Merck, USA).

4.4 *In vitro* release study

The release of PTX from liposomes was investigated using the dialysis bag diffusion method. Briefly, 1 mL of PTX formulation was placed into a pretreated dialysis bag (MWCO 7000) and tightly sealed. Then, the container was immersed in 30 mL of PBS (pH 7.4) containing 20% (v/v) ethanol and incubated with gentle shaking (100 rpm) for a 60 h period at 37 ± 0.5 °C. Samples (100 μ L) were taken at predetermined time points from the release medium and replaced by an equivalent volume of fresh medium. The concentration of PTX was determined by HPLC at 227 nm after 10 min centrifugation at 8000 rpm without further treatment.

4.5 Cell culture

Human HeLa and MCF-7 cells were provided by American Type Culture Collection (ATCC, Manassas, USA) and cultured in DMEM medium containing 50 U per mL streptomycin, 100 U per mL penicillin and 10% fetal bovine serum (FBS, Sigma-Aldrich, St Louis, MO). The cells were cultured at 37 ± 0.1 °C in a humidified incubator with $5 \pm 0.1\%$ CO₂ and hypoxia incubator (Ruskin Invivo₂ 1000, Bridgend, UK) with 0.1% oxygen. All the cell cultures were maintained in 25 cm² or 75 cm² cell culture flasks. Subculture: the cells were passaged at 70–80% confluent with trypsin and medium every 2 to 3 days.

4.6 Cellular uptake and delivery

The uptake process was observed by confocal laser scanning microscopy (CLSM). For the microscopic analysis, liposomes loaded with GAPDH-siRNA (mixed with 10% Alexa Fluor®647 labelled siRNA as a fluorescent probe) and PTX (mixed with 10% coumarin-6 as a fluorescent probe) were used. HeLa cells were cultured on round glass coverslips in 24-well plates (5×10^4 cells per well). After washing three times with PBS, different formulations were added to the corresponding wells. After an incubation period of 4 h, the cells were washed three times with ice cold PBS and fixed with 4% formaldehyde for 20 min at room temperature, and the nuclei were stained with DAPI. Finally, the fixed cell slides were visualized with a Nikon C2SI microscope (Nikon, Japan).

Potential endocytic pathways of PEGylated liposomes were studied by HeLa cells based on the liposome formulation with siRNA-PTX/coumarin-6. As the inhibitors of different uptake pathways, sodium azide (3 μ g mL⁻¹), chlorpromazine (10 μ g mL⁻¹), quercetin (6 μ g mL⁻¹), indomethacin (6 μ g mL⁻¹) and colchicine (8 μ g mL⁻¹) were added into each well and pre-incubated for 1 h, respectively. Thereafter, the cells were treated by liposomes containing 3 μ g mL⁻¹ coumarin-6. After 2 h culture with inhibitors, the cells were washed, harvested and analyzed by using an FACS Calibur flow cytometer (BD Company, Sparks, USA).

4.7 Cell transfection and the GAPDH test

One day before transfection, 8000 cells were plated in 100 μ L of growth medium without antibiotics in each well at a 96-well format under normal and hypoxic culture conditions. The cell density reached 30–50% confluency at the time of transfection. GAPDH-siRNA and Lipofectamine™ 2000 (dose as 0.15 μ L per 10 nM siRNA) were gently diluted in 50 μ L Opti-MEM® (I Reduced Serum Medium without serum). The diluted siRNA was combined with diluted Lipofectamine. This was mixed gently and incubated for 10–20 min at 25 °C. The liposomes loaded with GAPDH-siRNA or negative control siRNA were prepared as described in section 4.2, added to the cells (final siRNA concentration was 10, 25, 50 and 100 nM) and incubated for 4 h at 37 °C under a 5% CO₂-containing atmosphere. The cells were replaced with fresh full medium and further incubated for 44 h. Lipofectamine 2000 (dose as 0.15 μ L per 10 nM siRNA) was applied as positive control.

After removing the culture medium from the transfected cells, the total protein test (MicroBCA assay) was performed using a Thermo Scientific MicroBCA™ Protein Assay Kit (Rockford, USA). 200 μ L KDAlert™ lysis buffer was added to each sample well. After incubation at 4 °C for 20 min, the cell lysate was pipetted up and down 5 times. 10 μ L of the sample was transferred to a 96-well plate. 90 μ L of KDAlert™ Master Mix was added to each sample. The increase in fluorescence ($\lambda_{\text{excitation}} = 545$ nm; $\lambda_{\text{emission}} = 575$ nm) was measured at room temperature. The GAPDH activity of the different samples could be compared by using their increase in fluorescence value (per μ g total protein). If GAPDH is silenced, the increased value will diminish.

4.8 *In vitro* cytotoxicity assay

The effect of Taxol, siRNA lipoplexes and siRNA-PTX liposomes on the visibility of MCF-7 and HeLa cells was examined using the Promega CellTiter 96® AQueous One Solution Cell Proliferation (MTS) assay. Cells were seeded in 96-well plates in DMEM medium with 10% FBS. After the indicated treatment and incubation period, the MTS-labeling reagent was added, and the spectrophotometric absorbance of the samples was measured on a microplate reader at 490 nm. Each treatment was performed in triplicate.

4.9 Animals and the tumor xenograft model

Female BALB/c nude mice (4–6 weeks old; weight at 18–22 g) were purchased from Beijing HFK Bioscience Co., Ltd. All animal studies were carried out in compliance with the guidelines outlined in the Guide for the Care and Use of Laboratory. All animal experiments were approved by the Animal Experiment Ethics Committee of Shenyang Pharmaceutical University.

The tumor xenograft model was established by subcutaneously injecting 5×10^6 HeLa cells in normal saline into the armpit region of the mice. The tumor diameters were measured with callipers every 3 days, and tumor volumes were calculated as $V = \text{width}^2 \times \text{length}/2$. After 2 weeks post-tumor inoculation, tumor volumes reached around 100 mm^3 .

4.10 *In vivo* targeting assay

For targeting the formulations *in vivo*, the near infrared fluorescence dye DiR was applied to investigate the biodistribution and targeting ability in living animals. BALB/c nude mice with subcutaneous tumors of approximate 100 mm^3 were subjected to tail vein injection of PTX-DiR (w/w, 9:1) solution and liposomes at 3 mg kg^{-1} . Whole-body fluorescence images were recorded at 2, 4, 8, 12, and 24 h after intravenous administration through Caliper LifeSciences LIVIS® Lumina Series III (PerkinElmer, MA, USA) with the following parameters for DiR: $\lambda_{\text{excitation}} = 745 \text{ nm}$; $\lambda_{\text{emission}} = 800 \text{ nm}$. *In vivo* images of the excised organs and tumors were obtained at 24 h post injection.

4.11 RBCs safety evaluation

The hemolysis assay was used to select a suitable concentration of formulations. The rabbit red blood cells (RBCs) were collected at 1000 rpm for 10 min and washed with saline three times. The RBCs were diluted with saline to a concentration of 2% (v/v). Then 2 mL of Taxol® and PTX liposomes were added into an equal volume of RBC solutions, respectively, and the final PTX concentrations of the formulations were 0.6 and 0.3 mg mL^{-1} . The mixed solutions were kept static for 4 h. Subsequently, the mixtures were centrifuged, and the clear upper solutions were taken out and measured at 541 nm on a UV-vis spectrophotometer. The hemolysis of RBCs in distilled water and saline was used as the positive and negative controls, respectively. Hemolysis percentages (%) = $(\text{absorbances of the sample} - \text{absorbances of negative control}) / (\text{absorbances of the positive control} - \text{absorbances of negative control}) \times 100$. The different hemolysis percentages of the various concentrations of formulations were compared and finally a safe and appropriate concentration was selected for administration to the tumor xenograft nude mice.

4.12 *In vivo* antitumor efficacy test

The treatment of the tumor xenograft mice was initiated at a 48 h interval for 21 days. The mice were randomly divided into five groups ($n = 6$ per group) receiving different injections as follows: (1) normal saline (control), (2) siRNA liposomes, (3) Taxol®, (4) PTX liposomes, (5) siRNA-PTX liposomes. Tumor

volume ($V = \text{width}^2 \times \text{length}/2$) and body weight were recorded. After the last cycle of injection, the mice were sacrificed. The obtained tumors were accurately weighed to calculate the inhibition rate (TIR) by the following formula: $\text{TIR (\%)} = (W_{\text{control}} - W_{\text{sample}}) / W_{\text{sample}} \times 100$. Furthermore, tumor burden (%) was calculated as follows: the weight of tumors was divided by the average body weight of BALB/C nude mice $\times 100$.

4.13 Mechanisms involved in the reduction of tumors

4.13.1 ATP assay. HeLa cells were cultured in DMEM medium in 6-well plates (3×10^5 per well) under normal and hypoxic conditions for 24 h. Then the cells were treated with siRNA, PTX, siRNA-PTX and blank (control) liposomes for 4 h. The liquid was removed and 200 μL lysis buffer were added per well. After that, the cell lysate was centrifuged at $12\,000g$ at 4°C for 5 min. After BCA assay of the supernatant, intracellular ATP concentration was determined by using ATP luminescence determination kit with a SpectraMax M5 luminometer (Molecular Devices, Sunnyvale, USA) based on the normalised for total cell protein.

4.13.2 Western blotting analysis in autophagy and apoptosis. The protein assay was continued after the ATP assay. The supernate extracts (40 μg protein) were subjected to electrophoresis in SDS-PAGE on 10% gels, separated and transferred to polyvinylidene fluoride (PVDF) membranes. The targeted protein was blocked with 5% nonfat milk in TBST (10 mM Tris-HCl, 150 mM NaCl and 0.05% Tween-20) for 1 h and incubated with primary antibody to caspase-3, β -actin, Atg-5 and Atg-12 overnight at 4°C . After being washed with TBST 3 times, the membranes were incubated with goat anti-rabbit and anti-mouse IgG-HRP secondary antibody. Finally, bands were visualised by using the ECL reagent in a dark room. Then the photographic films with blots were scanned into PDF images and edited by image processing software (Adobe Illustrator) to crop the images to only show relevant slots. Photoshop was also used to increase the graphic contrast and invert the background colours of the blots.

4.14 Statistical analysis

All statistical analyses in this paper were performed using Student's *t*-test. The differences were considered significant at $*p < 0.05$, $**p < 0.01$, and $***p < 0.001$.

Acknowledgements

Jibin Guan is supported by a Ph.D. grant (CSC student no. 201408210111) from the China Scholarship Council. This work was financially supported by the National Nature Science Foundation of China (No. 81373336, 81573371).

References

- 1 M. M. Gottesman, T. Fojo and S. E. Bates, *Nat. Rev. Cancer*, 2002, 2, 48–58.

- 2 T. Minko, L. Rodriguez-Rodriguez and V. Pozharov, *Adv. Drug Delivery Rev.*, 2013, **65**, 1880–1895.
- 3 J. Kopecka, S. Porto, S. Lusa, E. Gazzano, G. Salzano, A. Giordano, V. Desiderio, D. Ghigo, M. Caraglia and R. G. De, *Oncotarget*, 2015, **6**, 31461–31478.
- 4 E. V. Batrakova, S. Li, W. F. Elmquist, D. W. Miller, V. Y. Alakhov and A. V. Kabanov, *Br. J. Cancer*, 2001, **85**, 1987–1997.
- 5 E. V. Batrakova, S. Li, A. M. Brynskikh, A. K. Sharma, Y. Li, M. Boska, N. Gong, R. L. Mosley, V. Y. Alakhov, H. E. Gendelman and A. V. Kabanov, *J. Controlled Release*, 2010, **143**, 290–301.
- 6 A. Colell, J. E. Ricci, S. Tait, S. Milasta, U. Maurer, L. Bouchier-Hayes, P. Fitzgerald, A. Guio-Carrion, N. J. Waterhouse, C. W. Li, B. Mari, P. Barbry, D. D. Newmeyer, H. M. Beere and D. R. Green, *Cell*, 2007, **129**, 983–997.
- 7 A. A. Mokhtarieh, S. Cheong, S. Kim, B. H. Chung and M. K. Lee, *Biochim. Biophys. Acta*, 2012, **1818**, 1633–1641.
- 8 U. Lungwitz, M. Breunig, T. Blunk and A. Gopferich, *Eur. J. Pharm. Biopharm.*, 2005, **60**, 247–266.
- 9 C.-F. Wang, Y.-X. Lin, T. Jiang, F. He and R.-X. Zhuo, *Biomaterials*, 2009, **30**, 4824–4832.
- 10 M. Gunther, J. Lipka, A. Malek, D. Gutsch, W. Kreyling and A. Aigner, *Eur. J. Pharm. Biopharm.*, 2011, **77**, 438–449.
- 11 K. M. Kitchens, M. E. El-Sayed and H. Ghandehari, *Adv. Drug Delivery Rev.*, 2005, **57**, 2163–2176.
- 12 G. Navarro and C. Tros de Ilarduya, *Nanomedicine*, 2009, **5**, 287–297.
- 13 M. Lavertu, S. Methot, N. Tran-Khanh and M. D. Buschmann, *Biomaterials*, 2006, **27**, 4815–4824.
- 14 S. Mao, W. Sun and T. Kissel, *Adv. Drug Delivery Rev.*, 2010, **62**, 12–27.
- 15 S. P. Strand, S. Lelu, N. K. Reitan, C. de Lange Davies, P. Artursson and K. M. Varum, *Biomaterials*, 2010, **31**, 975–987.
- 16 D. Schaffert and E. Wagner, *Gene Ther.*, 2008, **15**, 1131–1138.
- 17 K. A. Howard, *Adv. Drug Delivery Rev.*, 2009, **61**, 710–720.
- 18 H. Meng, M. Liong, T. Xia, Z. Li, Z. Ji, J. I. Zink and A. E. Nel, *ACS Nano*, 2010, **4**, 4539–4550.
- 19 P. R. Dash, M. L. Read, K. D. Fisher, K. A. Howard, M. Wolfert, D. Oupicky, V. Subr, J. Strohalm, K. Ulbrich and L. W. Seymour, *J. Biol. Chem.*, 2000, **275**, 3793–3802.
- 20 D. E. Owens, 3rd and N. A. Peppas, *Int. J. Pharm.*, 2006, **307**, 93–102.
- 21 M. Ogris, S. Brunner, S. Schuller, R. Kircheis and E. Wagner, *Gene Ther.*, 1999, **6**, 595–605.
- 22 P. Opanasopit, M. Nishikawa and M. Hashida, *Crit. Rev. Ther. Drug Carrier Syst.*, 2002, **19**, 191–233.
- 23 T. M. Sun, J. Z. Du, Y. D. Yao, C. Q. Mao, S. Dou, S. Y. Huang, P. Z. Zhang, K. W. Leong, E. W. Song and J. Wang, *ACS Nano*, 2011, **5**, 1483–1494.
- 24 Y. Wang, M. Saad, R. I. Pakunlu, J. J. Khandare, O. B. Garbuzenko, A. A. Vetcher, V. A. Soldatenkov, V. P. Pozharov and T. Minko, *Clin. Cancer Res.*, 2008, **14**, 3607.
- 25 T. Zhang, S. Zhou, L. Kang, X. Luo, Y. Liu, Y. Song, X. Liu and Y. Deng, *Asian J. Pharm. Sci.*, 2017, **12**, 134–142.
- 26 S. J. D. Amir Abbas Mokhtarieh and M. K. Lee, *Daru, J. Pharm. Sci.*, 2013, **21**, 32.
- 27 V. Filipe, A. Hawe and W. Jiskoot, *Pharm. Res.*, 2010, **27**, 796–810.
- 28 J. Dredán, I. Antal and I. Rácz, *Int. J. Pharm.*, 1996, **145**, 61–64.
- 29 T. Higuchi, *J. Pharm. Sci.*, 1963, **52**, 1145–1149.
- 30 U. S. Huth, R. Schubert and R. Peschka-Süss, *J. Controlled Release*, 2006, **110**, 490–504.
- 31 J. A. Swanson and C. Watts, *Trends Cell Biol.*, 1995, **5**, 424–428.
- 32 B. Bhattacharya, S. H. H. Low, C. Soh, N. Kamal Mustapa, M. Belouche-Babari, K. X. Koh, J. Loh and R. Soong, *Br. J. Pharmacol.*, 2014, **171**, 3255–3267.
- 33 M. R. Elliott, F. B. Chekeni, P. C. Trampont, E. R. Lazarowski, A. Kadl, S. F. Walk, D. Park, R. I. Woodson, M. Ostankovich, P. Sharma, J. J. Lysiak, T. K. Harden, N. Leitinger and K. S. Ravichandran, *Nature*, 2009, **461**, 282–286.
- 34 W. Zhang, Y. Shi, Y. Chen, S. Yu, J. Hao, J. Luo, X. Sha and X. Fang, *Eur. J. Pharm. Biopharm.*, 2010, **75**, 341–353.